Weierstraß-Institut
für Angewandte Analysis und Stochastik
Leibniz-Institut im Forschungsverbund Berlin e. V.

Preprint ISSN 2198-5855

The link between coherence echoes and mode locking

Sebastian Eydam, Matthias Wolfrum

submitted: June 11, 2019

Weierstrass Institute
Mohrenstr. 39
10117 Berlin
Germany
E-Mail: sebastian.eydam@wias-berlin.de
matthias.wolfrum@wias-berlin.de

No. 2596
Berlin 2019

2010 *Mathematics Subject Classification.* 34C15, 37N20.

2010 *Physics and Astronomy Classification Scheme.* 42.60.Fc, 05.45Xt, 05.45.-a.

Key words and phrases. Phase oscillators, mode-locking.

The authors acknowledge the support by Deutsche Forschungsgemeinschaft in the framework of Collaborative Research Center SFB 910.

Edited by
Weierstraß-Institut für Angewandte Analysis und Stochastik (WIAS)
Leibniz-Institut im Forschungsverbund Berlin e. V.
Mohrenstraße 39
10117 Berlin
Germany

Fax: +49 30 20372-303
E-Mail: preprint@wias-berlin.de
World Wide Web: http://www.wias-berlin.de/

The link between coherence echoes and mode locking

Sebastian Eydam, Matthias Wolfrum

Abstract

We investigate the appearance of sharp pulses in the mean field of Kuramoto-type globally-coupled phase oscillator systems. In systems with exactly equidistant natural frequencies self-organized periodic pulsations of the mean field, called mode locking, have been described recently as a new collective dynamics below the synchronization threshold. We show here that mode locking can appear also for frequency combs with modes of finite width, where the natural frequencies are randomly chosen from equidistant frequency intervals. In contrast to that, so called coherence echoes, which manifest themselves also as pulses in the mean field, have been found in systems with completely disordered natural frequencies as the result of two consecutive stimulations applied to the system. We show that such echo pulses can be explained by a stimulation induced mode locking of a subpopulation representing a frequency comb. Moreover, we find that the presence of a second harmonic in the interaction function, which can lead to the global stability of the mode-locking regime for equidistant natural frequencies, can enhance the echo phenomenon significantly. The non-monotonous behavior of echo amplitudes can be explained as a result of the linear dispersion within the self-organized mode-locked frequency comb. Finally we investigate the effect of small periodic stimulations on oscillator systems with disordered natural frequencies and show how the global coupling can support the stimulated pulsation by increasing the width of locking plateaus.

Since the pioneering work of Kuramoto, systems of globally coupled phase oscillators are a topic of extensive studies. They are able to describe synchronization processes that have applications in many fields, including e.g. neuronal systems, coupled Josephson junctions, or systems biology. Beyond the transition from incoherent to synchronized behavior such systems can display a variety of interesting dynamical regimes. In this paper, we study the emergence of sharp pulses in the mean field, which can be found as a collective dynamics already below the threshold for the onset of synchrony. Such pulses have been described to arise in a self-organized way if the natural frequencies are exactly equidistant. At the other hand, similar pulsations can be found as a transient dynamics in systems with completely random frequencies as the result of two consecutive stimulations applied to the system. These so called coherence echoes arise after a time distance equal to the distance between the two stimuli and show similarities to plasma echoes. We show here that these two phenomena have a common origin in a collective order of the phases of unsynchronized oscillators with exactly or nearly equidistant natural frequencies. A similar process in the nonlinear phase dynamics of optical systems is called mode locking. We describe the role of the underlying frequency combs and show how certain features of the nonlinear coupling of the phases can have an essential influence on the pulsation behavior.

DOI 10.20347/WIAS.PREPRINT.2596 Berlin 2019

1 Introduction

In the field of coupled oscillator systems, Kuramoto[1] made an important contribution to the understanding of collective phenomena, when he derived a model of globally-coupled phase oscillators with heterogeneous natural frequencies that exhibits a transition from incoherence to a state of partial collective synchrony above a critical coupling strength. Since then, the theory of synchronization of coupled oscillators has been an active area of research.[2] Before the onset of collective synchronization the typical dynamical behavior of globally-coupled phase oscillators is phase turbulence.[3] However, it could be shown that with equidistant natural frequencies another collective type of phenomenon exists called *mode locking*.[4, 5] Mode locking is a phenomenon which is particularly well known in the field of optics. Important recent developments include phase models that can be derived from the Lugiato-Lefever model.[6, 7]

Another interesting and seemingly unrelated phenomenon can be found by subjecting a system of phase oscillators with random natural frequencies in the incoherent regime to two external stimuli separated in time by an interval of length τ. It is then observed that echo-type responses in the mean field follow at integer multiples of τ.[8] Similar echo-type phenomena have been known in the field of plasma physics,[9, 10, 11] and as spin echoes in systems with nuclear magnetic dipoles in inhomogeneous external magnetic fields.[12, 13] Recent realizations of echo-type phenomena in oscillator systems were obtained for systems of stimulated chemical oscillators,[14] and for kicked rotators,[15].

The present work is organized as follows. After introducing in Sec. 2 the phase oscillator model, its mean field formulation, and the instantaneous stimuli, we show that self-organized mode locking can appear also for frequency combs with modes of finite width, where the natural frequencies are randomly chosen from equidistant frequency intervals. In Sec. 3 we elaborate on the relation between mode locking and coherence echoes. We show that the echo response is due a temporarily induced mode locking of a subpopulation of the oscillators with natural frequencies from a corresponding comb structure. This comb is selected by the stimulation and a specific initial state is induced, which is similar to the self-organized mode locking in systems with equidistant natural frequencies. We find that the second harmonic in the nonlinear global coupling of Kuramoto-Daido type, which has been shown to be the key ingredient for self-organized mode locking in [4], also has substantial influence on the amplitude of the stimulated pulses and explain the origin of non-monotonous echo amplitudes. Finally, in Sec. 4 we investigate the case of a periodic stimulation of phase oscillator systems with random frequencies. In this case there emerges already for small stimulations a state with pulsating mean field. We use the relationship to ensembles of circle maps in the coupling free limit to explain the basic structure of the average frequencies for this regime of stimulated mode locking. We summarize and discuss our findings in Sec. 5.

2 The Kuramoto-Daido Model below the Threshold of Synchronization

Our basic system of globally-coupled phase oscillators describing the dynamics of the phase variables $\theta_k \in S^1 = \mathbb{R}/2\pi\mathbb{Z}$, has the form

$$\dot{\theta}_k = \omega_k + \frac{K}{N}\sum_{j=1}^{N} f(\theta_j - \theta_k), \tag{1}$$

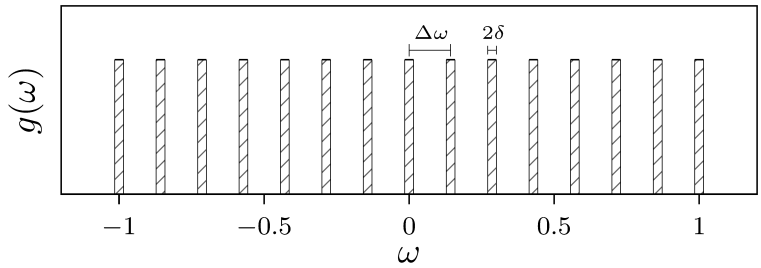

Figure 1: Comb-like frequency distribution $g(\omega)$, where ω_k are chosen with uniform probability from equidistant intervals $M_m = [m\ \Delta\omega - \delta, m\ \Delta\omega + \delta]$ with width $2\delta = 0.03$ and spacing $\Delta\omega = 1/7$.

where $k \in \{1, \ldots, N\}$ is the oscillator index, N is the total number of oscillators, ω_k are the natural frequencies, and K is the coupling strength. The interaction function $f(\cdot)$ for the global coupling in (1) is taken in the form

$$f(\theta_j - \theta_k) = \gamma \sin(\theta_j - \theta_k) + (1-\gamma)\sin(2(\theta_j - \theta_k)), \tag{2}$$

where $\gamma \in [0, 1]$ is used to balance the two Fourier modes in $f(\cdot)$ while keeping the total amount of coupling fixed. The global coupling can be expressed in terms of the corresponding two complex Kuramoto-Daido order parameters[16], given for $q \in \{1, 2\}$ as

$$\eta_q(t) = R_q(t)e^{\mathrm{i}\Psi_q(t)} := \frac{1}{N}\sum_{j=1}^{N} e^{\mathrm{i}q\theta_j(t)} \in \mathbb{C}. \tag{3}$$

They can be used to rewrite (1) as

$$\dot{\theta}_k = \omega_k - K\left[R_1\gamma\sin(\theta_k - \Psi_1) + R_2(1-\gamma)\sin(2\theta_k - \Psi_2)\right] \tag{4}$$

such that the interaction is transformed into a coupling of every oscillator with only the two global order parameters (3). The presence of higher Fourier harmonics in the interaction function has been found in the phase response of e.g. weakly-coupled Hodgkin-Huxley neurons[17] and their impact on the phase dynamics has been studied extensively [16, 18, 19]. For non-identical natural frequencies ω_k, e.g. from a uniform or Gaussian distribution there is a threshold K_C for the onset of synchronization. A comprehensive theory based on a center manifold reduction for the onset of collective synchronization in the continuum limit $(N \to \infty)$ of this particular system has been recently presented by Chiba [20]. The typical behavior of the system (1) in the regime $K < K_C$ is phase turbulence. However, for equidistant natural frequencies $\omega_{k+1} - \omega_k = \Delta\omega$ a new collective dynamical regime, called *mode locking*, has been reported [4], which exists below the synchronization threshold K_C and is characterized by sharp periodic pulses in the mean field $R_1(t)$. Another interesting behavior of system (1) below the synchronization threshold and for random natural frequencies are so called *coherence echoes*, which were studied in [8]. These echoes manifest themselves also as sharp peaks in the mean field, in this case induced by a stimulation applied to the system. The specific feature of the coherence echoes is that the peaks appear not only directly induced by a stimulus, but after the application of two stimuli there may appear further "echo" pulses at a time distance of the original two stimuli. Below, we will describe these two phenomena in more detail and discuss their connection.

Mode Locking

While the mechanism of mode locking is a well established technique to achieve short pulses in optical systems, a similar mechanism in globally coupled phase oscillators has been described only recently

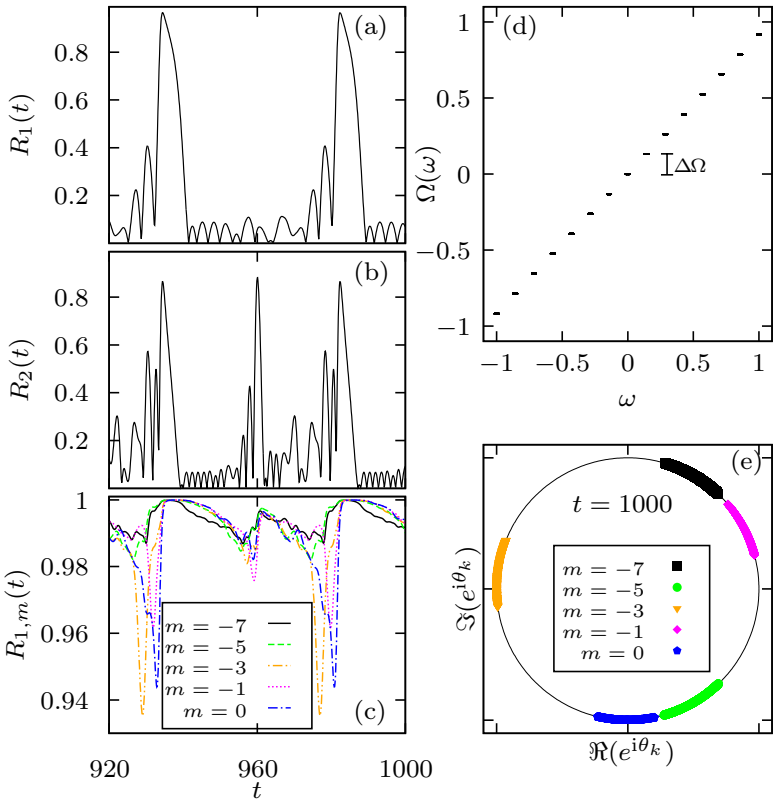

Figure 2: (Color online) Self-organized mode-locked state in system (4) with $(K, \gamma) = (1.2, 0.7)$. Natural frequencies from distribution in Fig. 1 with $N_M = 10^3$ oscillators in each subinterval (5). Panel (a)–(c): time traces $R_1(t)$, $R_2(t)$ and $R_{1,m}(t)$ for $m \in \{-7, -5, -3, -1, 0\}$ (d): comb of effective $\Omega_k(\omega_k)$ Panel (e): a snapshot of the phases at $t = 1000$ with the same coloring for the different modes as in (c).

[4]. It was found that although stable mode-locking can be obtained for specific initial conditions already for the classical case of Kuramoto coupling $\gamma = 1$, the presence of a second harmonic in the interaction function (2) can transform it into a self-organized globally stable dynamical regime. While the results in [4] were restricted to the case of exactly equidistant natural frequencies, we will show here that stable mode-locked solutions can also appear in large populations of phase oscillators, with natural frequencies chosen randomly from a comb like distribution (cf Fig. 1). To this end, we define a set of equidistant disjoint frequency intervals

$$M_m = [m\ \Delta\omega - \delta, m\ \Delta\omega + \delta], \tag{5}$$

where $m \in \{-n, \ldots, n\}$ is called the mode index, $2n + 1$ is the number of intervals, $\Delta\omega \in \mathbb{R}^+ = 1/n$ is the equidistant spacing between centers of the intervals, and 2δ is the width of each interval with $2\delta < \Delta\omega$. The natural frequencies are then drawn with uniform probability from the union of the intervals $M = \cup_m M_m$. An example of such a distribution of natural frequencies for $2n + 1 = 15$ and $2\delta = 0.03$ is depicted in Fig. 1.

For $\delta > 0$ the mode locking becomes a two-stage process, where at first the oscillators within the frequency interval M_m become synchronized. The entrainment among the oscillators with $\omega_j \in M_m$ can be seen by employing so-called modal order parameters given by

$$R_{1,m}(t)e^{\mathrm{i}\Psi_{1,m}(t)} := \frac{1}{N_m} \sum_{j \text{ if } \omega_j \in M_m} e^{\mathrm{i}\theta_j(t)}, \tag{6}$$

where N_m is the number of oscillators with $\omega_j \in M_m$. The mutual entrainment among the oscillators belonging to an interval M_m means that their effective frequencies

$$\Omega_k := \lim_{t\to\infty} \frac{1}{t} \int_0^t \dot{\theta}_k(\tau) d\tau = \lim_{t\to\infty} \frac{\tilde{\theta}_k(t) - \tilde{\theta}_k(0)}{t}, \tag{7}$$

where $\tilde{\theta}_k$ refers to the phase lifted to $\mathbb{R}$, become identical.

These collective effective frequencies Ω_m resulting from the locking within each interval M_m are equidistant and allow now for the mode locking of the collective modes formed by each frequency interval as described in [4]. The resulting periodic pulses in the mean field are a consequence of nearly identical phases of the collective modes, reappearing after a different number of round trips for each mode performed during the time $T = 2\pi/\Delta\Omega$, given by the spacing of the effective frequencies.

An explicit example of such a mode locking is shown in Fig. 2, where we took $N_m = 10^3$ oscillators with independent random uniform natural frequencies within each M_m from the frequency distribution $g(\omega)$ depicted in Fig. 1. Choosing the parameters $(K, \gamma) = (1.2, 0.7)$, which according to [4] are favorable for globally stable mode locking, we obtain a trajectory with typical sharp pulses in $R_1(t)$, $R_2(t)$, see Fig. 2 (a)–(b). The effective frequencies in panel (d) show a complete locking within each mode, while the time traces $R_{1,m}(t)$ in Fig. 2 (c) exhibit a periodic breathing behavior. This results from a different spreading of the phases within each mode shown by different colors in panel (e). Note that for stable self-organized mode locking the spacing of the effective frequencies

$$\Delta\Omega = \Omega_{m+1} - \Omega_m$$

is always slightly bigger than the spacing $\Delta\omega$ in the comb of the natural frequencies. The mode locking for such a distribution of natural frequencies will be used later to explain the repetitive pulses in a system with natural frequencies uniformly distributed within a single interval, where a self-organized subpopulation of oscillators with frequencies within a comb structure (5) can be responsible for the pulsating mean field.

3 Coherence Echoes and their relation to mode locking

The echo phenomenon in globally coupled oscillator systems that was found in[8] is now studied for systems of the form (1) with completely random natural frequencies, chosen uniformly distributed within an interval. Applying two consecutive stimuli with a time distance τ, the system can respond with one or several echo pulses, separated again by the time distance τ.

Following[8, 14] one uses instantaneous stimuli to transform the system state at a time moment t_p according to the rule

$$\theta_k(t_p^+) = \theta_k(t_p^-) - h(\theta_k(t_p^-)), \quad k \in \{1, \dots, N\}, \tag{8}$$

where t_p^- and t_p^+ denote the times directly before and directly after the stimulus, and $h(\cdot)$ is the stimulus action function.

We consider two different types of stimuli in this paper, the first one $h_1(\cdot)$ is continuous and similar to the one used by Ott et al. [8]

$$h_1(\theta) = \varepsilon(\alpha \sin(\theta) + (1-\alpha)\sin(2\theta)), \tag{9}$$

where ε is the stimulus strength and $\alpha \in [0, 1]$ is a parameter balancing between the two harmonics. A stimulus using (9) is referred to as an *impact stimulus*.

The second type $h_2(\cdot)$ to be considered, is a phase resetting stimulus that resets all phases within a small interval of length 2ρ identically to zero

$$h_2(\theta) = \begin{cases} \theta, & |\theta| \leq \rho, \\ 0, & |\theta| > \rho. \end{cases} \tag{10}$$

A similar type of stimulus has been argued to be valid in the context of chemical oscillators.[14] The action function (10) is discontinuous with an action of "all-or-nothing" type. It is called a *reset stimulus*. I turns out that the two different stimulus action functions (9) and (10), are both able to induce an echo-type response.

We consider the coherence echo phenomenon for a large population of phase oscillators of $N = 10^6$, whose natural frequencies are independent randomly distributed according to a uniform density within the interval $[-1, 1]$. Stimuli are applied at the times $t_1 = 30$ and $t_2 = 60$, resulting in an interstimulus interval of $\tau = t_2 - t_1 = 30$. To give an example, we take the stimulus of impact type (9) with $(\varepsilon, \alpha) = (1/2, 1/2)$ and fix the parameters of the oscillator system to $(K, \gamma) = (1.2, 0.7)$, which are the same parameters that were previously found to support stable mode locking. The time trace $R_1(t)$ presented in Fig. 3 (a) shows an echo response appears at time $t_3 = t_2 + \tau$. In Fig. 3 (b)–(d) we present snapshots of (θ_k, ω_k) at the times t_1^+, t_2^+, and t_3. For a better understanding of the echo mechanism, we arrange the oscillators into four groups, depending on how they are affected by each stimulus. Let $\theta_{\max} \in (0, \pi]$ be the angle at which (9) takes its maximum. The oscillators with $|\theta_k(t^-)| \leq \theta_{\max}$ at the time t^- immediately before a stimulus will be most strongly affected by the stimulus. Accordingly, for the snapshot at t_1^+ the strongly affected oscillators with $\left|\theta_k(t_1^-)\right| \leq \theta_{\max}$ are colored in red and the rest in gray. After the second stimulus, oscillators strongly affected also by the second pulse are changed to black, while those affected only by the second stimulus are now purple. A density plot taken over the population of black oscillators at time $t = t_2+$ highlights the increased density of oscillators on a frequency comb, see Fig. 3 (e).

The frequencies of the black subpopulation, selected by the two stimuli of time distance τ, belong to a sequence of equidistant intervals in ω as given in (5), Comparing panels (b) and (c), one can observe that the number of round trips performed by oscillators from neighboring subintervals differs by approximately one. Hence, the spacing of the subintervals is related to the time difference of the stimuli τ in the same way as the mode spacing to the pulse period $T = 2\pi/\Delta\Omega$ in the mode locking discussed before. The width 2δ of the subintervals is given by our choice $|\theta_k(t^-)| \leq \theta_{\max}$ for the different coloring of the oscillators. Note that the black oscillators at $t = t_2^+$ after the second stimulus have nearly identical phases. The final snapshot at the time of the echo $t = t_3$ shows that the black population reappears aligned in phase again but less focused, resulting in a slightly smaller echo response. Hence, the subpopulation of black oscillators shows a mode-locked behavior. However, due to the presence of the other oscillators, which behave incoherently and do not contribute to the mean field pulses, the nonlinear coupling is not strong enough to sustain the mode locking and the pulses decay. A detailed analytical investigation in form of an amplitude expansion of the order parameter has been carried out by Ott et al. [8] where the time of the echo is predicted and the influence of higher harmonics in the stimulus function is also discussed.

A second example, employing the reset stimulus (10) with $\rho = \pi/2$ is presented in Fig. 4. Here, the time traces $R_1(t)$, $R_2(t)$ in response to the stimuli, result in a sequence of multiple echoes of varying magnitudes, cf. Fig. 4 (a). In particular, one observes that the third echo is smaller than the fourth, i.e. a nonmonotonic behavior of the echoes. Besides the indicated echoes in $R_1(t)$, intermediate pulses of

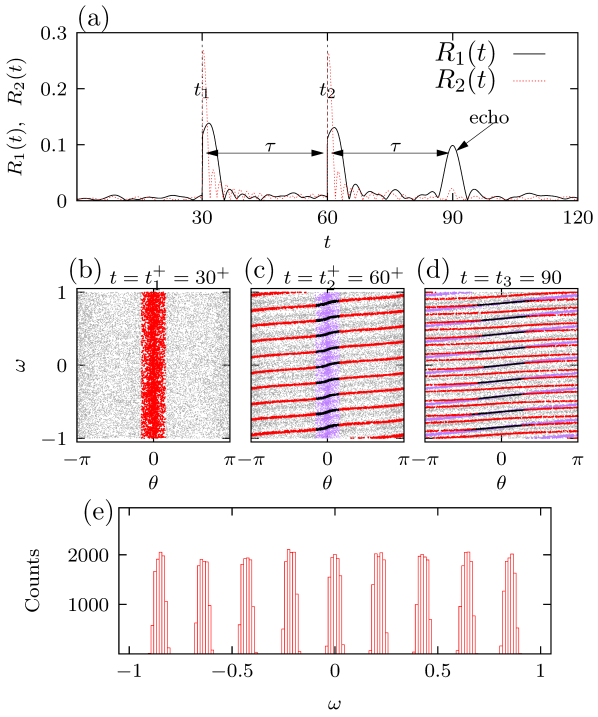

Figure 3: (Color online) Coherence echoes in system (4) with $(K, \gamma) = (1.2, 0.7)$ stimulated by impact stimuli (9) with $(\varepsilon, \alpha) = (1/2, 1/2)$ at $t_1 = 30$ and $t_2 = 60$, for $N = 10^6$ oscillators initialized at random. Panel (a): time traces $R_1(t)$, $R_2(t)$; (b)–(d): snapshots of distribution of phases θ_k versus natural frequencies ω_k at times t_1^+, t_2^+, and $t_3 = t_2 + \tau$. The explanation of the coloring in (b)–(d) is given in the text. (e): histogram of natural frequencies of the black subpopulation.

$R_2(t)$, for instance, at $t = t_2 + \tau/2$ are present. This is a feature that is also typically found in mode-locked solutions, cf. Fig. 2 (b). The coloring of the snapshots in Fig. 4 (b)–(d) at the times t_1^+, t_2^+, and $t_3 = t_2 + \tau$ follows the same scheme as before using now the reset threshold $\left|\theta_k(t_{1,2}^-)\right| \leq \rho$. Oscillators being reset by the first stimulus are red, those reset by the second stimulus are purple, and those reset by both stimuli are black. With the reset stimuli, completely empty regions appear after stimulation and in the stimulated comb (black) all the phases are exactly identical at t_2^+. Here, the width 2δ of the subintervals for the mode-locked subpopulation results directly from the reset threshold ρ. To illustrate the comb structure that is generated by the second stimulus at $t = t_2^+$, we additionally supply a histogram plot over all $\theta_k(t_2^+) \approx 0$, see Fig. 4 (e).

We will study now several properties of the coherence echoes in more detail. Note that the coherence echoes appear already on the linear level, i.e. by stimulating a population of uncoupled oscillators. However, as we will show, the effect is strongly enhanced by the nonlinear coupling. At the other hand, the effect of nonmonotonic behavior of the echoes can be explained already on the linear level. To this end, we will also introduce synthetic mode-locked initial conditions, which mimic the result of the stimulation and generate the coherence echoes directly.

3.1 Impact of the nonlinear coupling

To investigate the impact of the second harmonic coupling, we perform the simulations of the echoes for the same stimuli that were used in Fig. 3 and Fig. 4 for varying γ. Instead of comparing the maxima of the first echoes E_1 directly, we present the relative echo strength scaled to the maximum in S_1 that

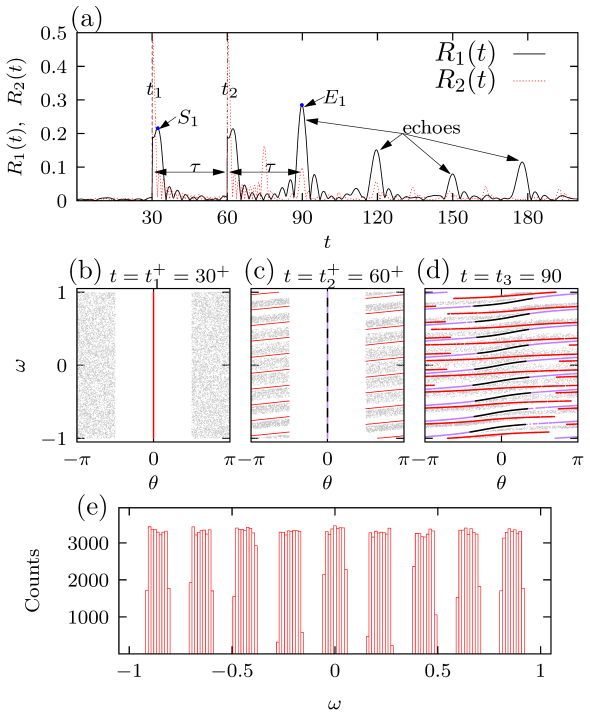

Figure 4: (Color online) Coherence echoes in system (4) with $(K, \gamma) = (1.2, 0.7)$ stimulated by reset stimuli (10) with $\rho = \pi/2$ at $t_1 = 30$ and $t_2 = 60$, for $N = 10^6$ oscillators initialized at random. Panel (a): time traces $R_1(t)$, $R_2(t)$; (b)–(d): snapshots of distribution of phases θ_k versus natural frequencies ω_k at times t_1^+, t_2^+, and $t_3 = t_2 + \tau$. The explanation of the coloring in (b)–(d) is given in the text. (e): histogram of natural frequencies of the black subpopulation.

occurs shortly after the first stimulus, which is important because changing γ affects the S_1. The two values S_1 and E_1 are indicated in the time trace $R_1(t)$, see Fig. 4 (a). The simulations are performed for different random initial conditions, system sizes $N = 10^6, 10^7$, and the results are shown in Fig. 5. Independent of the stimulus type, we find an increase of the echo magnitude for $\gamma < 1$, cf. (a)–(b) Fig. 5. Especially, one sees a wide range of parameter values for the stimulus h_2 with $\rho = \pi/2$, where E_1 becomes even larger than S_1, see Fig. 5 (b). We conclude from the simulations that the properly chosen second harmonic coupling enhances the echo effect significantly.

3.2 Synthetic Mode-Locked Initial Condition

Instead of generating echoes by two subsequent stimuli as in [8], we define now what we call a *mode-locked initial condition*

Definition 1. *For a set of* $2n + 1$ *equidistant frequency intervals* M_k *with spacing* $\Delta\omega$ *and widths* 2δ *given by* (5) *a corresponding mode-locked initial condition is given by*

$$\theta_k(0) = \begin{cases} 0, & \text{for} \quad \omega_k \in M := \cup_{m=-n}^{n} M_m \\ \theta_k \in [-\pi, \pi], & \text{uniform}, \end{cases} \tag{11}$$

where $k \in \{1, \ldots, N\}$ *is the oscillator index.*

Note that for such initial conditions, see Fig. 6, the modal order parameters (6) for the subintervals $R_{1,m}(0) = 1$ for all $m = -n, \ldots, n$, which is different to the situations after two stimuli where there

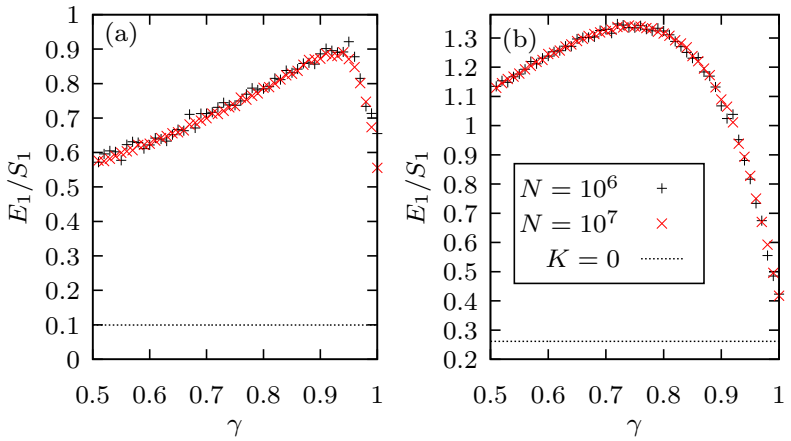

Figure 5: (Color online) Relative amplitudes E_1/S_1 of the first coherence echo for varying second harmonic coupling γ in system (4) with $K = 1.2$. (a): impact stimuli (9) with $(\varepsilon, \alpha) = (1/2, 1/2)$; (b): reset stimuli (10) with $\rho = \pi/2$. Dashed line: relative amplitudes E_1/S_1 without coupling $(K = 0)$.

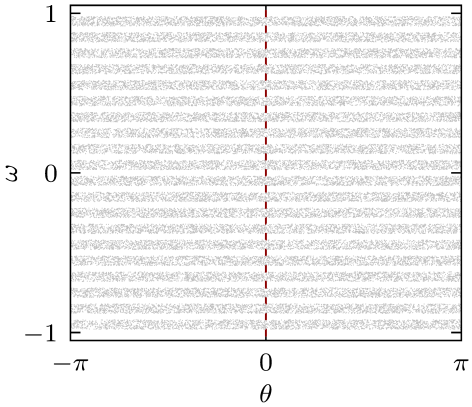

Figure 6: (Color online) Mode-locked initial condition (11) on equidistant frequency intervals (5) with $\Delta\omega = 0.1$ and $\delta = 0.02$.

are still incoherent oscillators with frequencies $\omega_k \in M$ that have not been affected by the stimuli such that the corresponding modal order parameters are smaller than one.

3.3 The nonmonotonicity of the echo magnitudes

We will show now that the nonmonotonous behavior of the magnitudes of the echoes, demonstrated in Fig. 4 (a), can be explained already in the uncoupled system $K = 0$ using the synthetic mode-locked initial conditions (11). To this end we calculate for $K = 0$ the mean field $R_1(t)$ explicitly in the continuum limit $N \to \infty$. Without coupling, one can compute separately the evolution of the modal order parameters for each of the intervals M_m as

$$R_{1,m}(t)e^{\mathrm{i}\Psi_{1,m}(t)} = \int_{-\infty}^{\infty} d\omega \int_0^{2\pi} e^{\mathrm{i}\theta} F_m(\theta, \omega, t) d\theta, \tag{12}$$

where $F_m(\theta, \omega, t)$ is the distribution function for the oscillators belonging to the mth frequency interval M_m. Integrating over θ we obtain the time independent uniform frequency distribution

$$\int_0^{2\pi} F_m(\theta, \omega, t) d\theta = g_m(\omega), \tag{13}$$

which in normalized form is given as

$$g_m(\omega) = \begin{cases} \frac{1}{2\delta}, & \text{for} \quad \omega \in M_m, \\ 0, & \text{else}, \end{cases} \tag{14}$$

where 2δ is the width of the interval M_m. In the continuum limit the mode-locked initial data $\theta_k(0) = 0$ for all oscillators with $\omega_k \in M_m$ is represented as a delta distribution and one can immediately write down its time evolution on the universal cover $\tilde{\theta} \in \mathbb{R}$ as

$$\tilde{F}_m(\tilde{\theta}, \omega, t) = \begin{cases} \frac{g_m(\omega)}{2\delta t}, & \text{for } \tilde{\theta} \in I(t) \\ 0, & \text{else}, \end{cases} \tag{15}$$

with the time dependent interval

$$I(t) = [(m\ \Delta\omega - \delta)t, (m\ \Delta\omega + \delta)t].$$

Now one can perform the integration in (12), which leads to the following expression for mth complex modal order parameter

$$R_{1,m}(t)e^{\mathrm{i}\Psi_{1,m}(t)} = \int_{-\infty}^{\infty} d\omega \int_{\tilde{\theta}\in I(t)} e^{\mathrm{i}\tilde{\theta}} \frac{g_m(\omega)}{2\delta t} d\tilde{\theta} = \frac{1}{2\delta t} \frac{1}{\mathrm{i}} \left[e^{\mathrm{i}(m\ \Delta\omega + \delta)t} - e^{\mathrm{i}(m\ \Delta\omega - \delta)t} \right]. \tag{16}$$

To obtain $R_1(t)$ for the continuum limit of the mode-locked initial condition, one can now combine the expressions (16) for all different $m \in \{-n, \ldots, n\}$ leading to

$$R_1(t)e^{\mathrm{i}\Psi_1(t)} = \frac{R_1(0)}{2n+1} \frac{\sin(\delta t)}{\delta t} \sum_{m=-n}^{n} e^{\mathrm{i}m\Delta\omega t}, \tag{17}$$

where $R_1(0)$ denotes the value of the mean field amplitude of the initial condition. While the summation in the last term provides the mode locking pulses at $p = 2\pi p/\Delta\omega$ for all $p \in \mathbb{N}$, we obtain also a periodically modulated envelope from the term $\sin(\delta t)$ and a decay of the order $1/t$. Each time the modulation term changes its sign, the phase of the pulses switches between 0 and π and at resonances between the switching and the pulsation frequency, the pulses will be completely suppressed.

In Fig. 7 we show the time traces of the global order parameters $R_1(t)$, $R_2(t)$ and a few selected modal order parameters, starting from a mode-locked initial condition with $(\Delta\omega, \delta) = (0.1, 0.02)$, where the distribution of the natural frequencies is taken to be uniform, covering the interval $[-1.02, 1.02]$. In this case, we see the fourth echo pulse with an increased amplitude and the fifth echo pulse completely suppressed. This mechanism can lead to non-monotone echo amplitudes also in the nonlinear case. Fig. 8 shows the time evolution starting from the same mode-locked initial condition (11) with $(\Delta\omega, \delta) = (0.1, 0.02)$ now using the coupling parameters $(K, \gamma) = (0.95, 0.7)$, which support mode locking for equidistant natural frequencies and strongly enhance the echo amplitudes. Again, the amplitude of the echo pulses is modulated by the dispersion induced slow oscillations of the modal order parameters. In contrast to the linear scenario in Fig. 7 we observe a sudden increase of all the modal order parameters at the first and second echo. The effects of nonlinear dispersion are especially pronounced for modes with high index $m = -10$ and result in different decay behavior of the modal order parameters. Moreover, we see an almost complete suppression of the third echo even though the modal order parameters still show considerable magnitudes. This can be explained by the effect of the first and second echo on the incoherent oscillators, which are not mode-locked in the initial condition. Note that the complement $\hat{M}$ of M consists of frequency intervals with the same spacing $\Delta\omega$

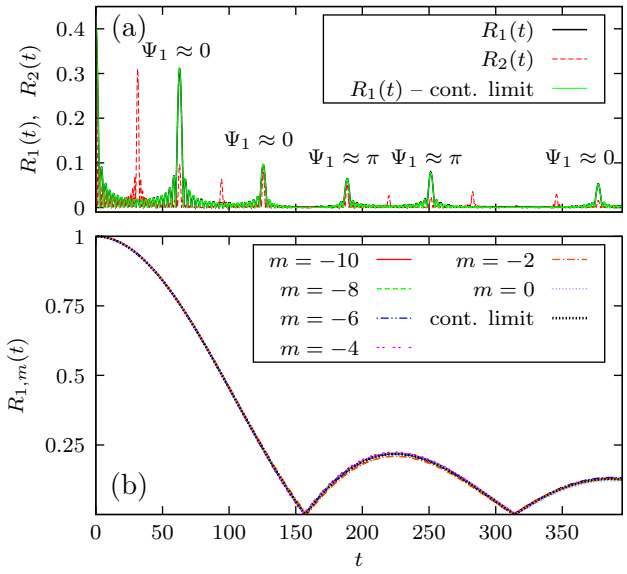

Figure 7: (Color online) Non-monotonous echo amplitudes in system (4) with $K = 0$ and mode-locked initial condition (11) with $(\Delta\omega, \delta) = (0.1, 0.02)$ and $N = 10^6$. (a)–time traces of the order parameters R_1, R_2, (b)–time traces of the modal order parameters and $R_{1,m}$ for selected mode numbers $m \in \{-10, -8, -6, -4, -2, 0\}$ together with corresponding time traces from the continuum limit (17) and (16).

and widths $2\hat{\delta} = \Delta\omega - 2\delta$. The echo pulses in the mean field induce a mode-locked pulsation also for this subpopulation of oscillators. These pulses have alternating phases, such that they alternatingly interfere constructively and destructively with the pulses from the initially mode-locked population. In the given example, this leads to a cancellation at the third echo. In Fig. 8(c) we show the time traces order parameters of the corresponding subpopulations

$$R_M(t) = \frac{1}{N_M}\left|\sum_{\omega_k \in M} e^{i\theta_k}\right| \quad \text{and} \quad R_{\hat{M}}(t) = \frac{1}{N_{\hat{M}}}\left|\sum_{\omega_k \in \hat{M}} e^{i\theta_k}\right|, \tag{18}$$

here N_M and $N_{\hat{M}}$ are the sizes of the two subpopulations.

4 Stimulated Mode Locking

The present section is concerend with the effects of periodic stimulation to a population of oscillators with random frequencies. The stimulated pulsed solution that arises will be referred to as a *stimulated mode-locked state*. The periodic stimulation is implemented in form of a stimulus train by applying the mapping of the phases (8) with impact or reset stimuli periodically at the times $t = p\tau = t_p$ with $p \in \mathbb{N}$.

We find that with the periodic stimulation a mode-locked frequency comb emerges. The locking is a gradual process which is especially pronounced for the reset stimulus type. The gradual increase of the stimulated pulses for reset stimuli of a particularly small reset range $\rho = \pi/8$, is presented in Fig. 9. The time trace $R_1(t)$ are plotted and the stimulus times t_p are indicated by dotted vertical lines, cf. Fig. 9 (a). One observes that the initial stimuli only have a small effect on $R_1(t_p^+)$, however, after multiple stimuli the response starts to increase until the mode-locking of the frequency comb is complete. The snapshots of the system at the times $t = t_5^+, t_{30}^+$ given in (b)–(c) Fig. 9, show that the

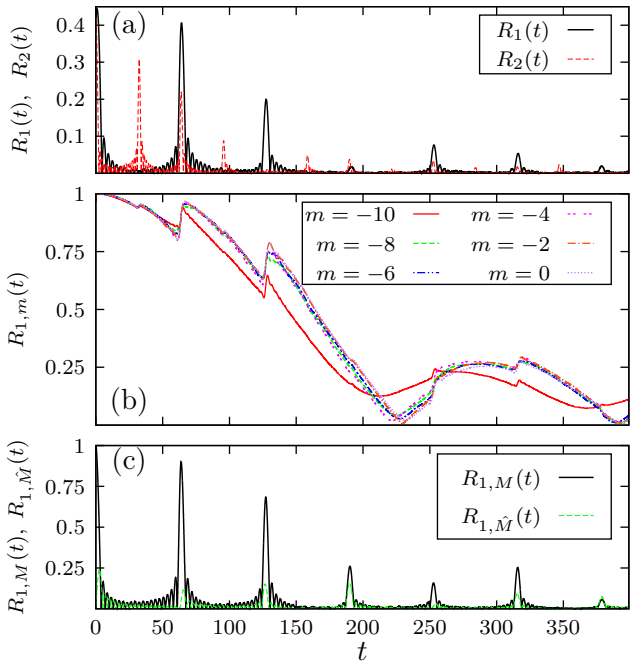

Figure 8: (Color online) Non-monotonous echo amplitudes in system (4) with $(K, \gamma, N) = (0.95, 0.7, 10^6)$ mode-locked initial condition (11) with $(\Delta\omega, \delta) = (0.1, 0.02)$. (a)–time traces of the order parameters R_1, R_2, (b)–time traces of the modal order parameters and $R_{1,m}$ for selected mode numbers $m \in \{-10, -8, -6, -4, -2, 0\}$, (c)–order parameters (18) for the comb M of the mode-locked initial condition and its complement $\hat{M}$.

increase of the stimulated pulsation is accompanied by the formation of desolated horizontal regions which correspond to a mode-locked frequency comb. In particular, for the reset stimulus this frequency comb is similar to the comb introduced in the mode-locked initial conditions Def. 1.

The impact stimuli, on the other hand, reach the final magnitude of the pulsation after fewer stimuli. An examples is given, where impact stimuli h_1 with $(\epsilon, \alpha) = (0.25, 1)$ are applied, cf. Fig. 10. Similarly, for the impact stimuli, horizontal desolated regions appear gradually, see Fig. 10 (b)–(c).

4.1 Periodic stimulation of uncoupled oscillators

For the decoupled oscillators with $K = 0$, one can reduce (1) with periodic stimulation to an ensemble of circle maps that give the phases $\theta_k(t_p^+)$ at the times immediately after the stimuli $t = (p\tau)^+ = t_p^+$

$$\theta_k(t_{p+1}^+) = \theta_k(t_p^+) + \omega_k\tau - h(\theta_k(t_p^+) + \omega_k\tau) \mod 2\pi. \tag{19}$$

Since $K = 0$ one can drop the oscillator index k an study the a single map of the type (19).

In the context of circle maps, the so-called *rotation number* $W(\omega)$, which gives the average number of rotations per iteration, is related to the effective frequency (7) in the time-continuous dynamics. If the following limit exists, the rotation number is given by

$$W\left(\omega, \tilde{\theta}(t_0^+)\right) := \lim_{p\to\infty} \frac{\tilde{\theta}(t_p^+) - \tilde{\theta}(t_0^+)}{2\pi p} = \Omega\left(\omega, \tilde{\theta}(t_0^+)\right) \frac{2\pi}{\tau}, \tag{20}$$

where $\tilde{\theta} \in \mathbb{R}$ denotes the phase variable lifted to the universal cover of S^1.

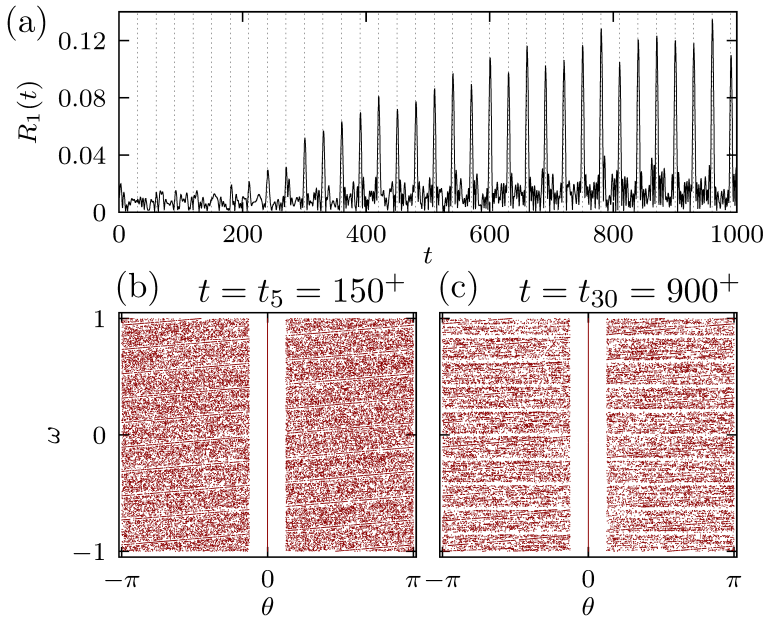

Figure 9: (Color online) Periodical stimulation of system (4) with $(K, \gamma, N) = (0.95, 2/3, 5 \cdot 10^4)$, random initial conditions, and reset stimuli h_2 with $\rho = \pi/8$ every $\tau = 30$ time units. (a)–time trace $R_1(t)$ together with vertical dotted lines indicating the stimulation times. (b), (c)–snapshots of the distributions at $t = t_5^+, t_{30}^+$ immediately after the stimuli.

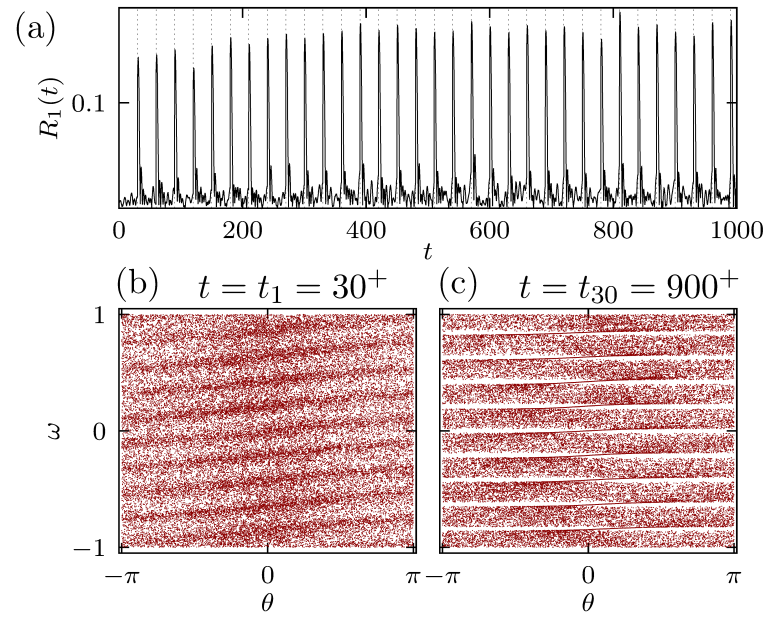

Figure 10: (Color online) Periodical stimulation of system (4) with $(K, \gamma, N) = (0.95, 2/3, 5 \cdot 10^4)$, random initial conditions, and impact stimuli h_1 with $(\epsilon, \alpha) = (0.25, 1)$ every $\tau = 30$ time units. (a)–time trace $R_1(t)$ together with vertical dotted lines indicating the stimulus times. (b), (c)–snapshots of the distributions at $t = t_1^+, t_{30}^+$ immediately after the stimuli.

Choosing $\alpha = 1$ for the impact stimuli (9), one obtains so-called *Arnold circle maps*. In this case, the rotation numbers (20) are independent of $\tilde{\theta}(t_0^+)$, strictly monotonously increasing with ω, and allow also for subharmonic locking to the forcing frequency for ω within the respective Arnold tongues.[21, 22] The range of the harmonic locking cones with integer rotation numbers giving $\Omega(\omega) = 2\pi z/\tau,\ z \in \mathbb{Z}$ is known to be bounded by $\omega = 2\pi z/\tau \pm |\varepsilon| /\tau$.[23]

In contrast to that, when using the reset stimuli (10), one obtains a discontinuous map. For some general results on the existence of the rotation number in circle maps with discontinuities the interested reader may be referred to Brette. [24] We find the ranges of the harmonic locking plateaus to be bounded by $\omega = 2\pi z/\tau \pm |\rho| /\tau$. Furthermore, in the case of the reset stimulus (10), we find that the rotation numbers are strictly rational multiples of the forcing frequency, which means that for any ω the orbit is periodic.

Theorem 4.1. *The circle map* (19) *with the stimulus action function* (10) *has a rational rotation number* (20) *for all* $\omega \in \mathbb{R}$.

Proof. For all $\omega \neq q\ 2\pi/\tau$ with $q \in \mathbb{Q}$ there is an iterate $p \in \mathbb{N}$ such that $\theta\left(t^+_{(p+1)}\right) = 0$ independent of the initial condition $\theta(t_0^+)$. This follows from the fact that a rigid rotation with an irrational rotation numbers covers S^1 uniformly. By the same argument, there will be another iterate at which the phase is once more mapped to zero. All other ω were already rational multiple of $2\pi/\tau$ by construction. □

We compute the effective frequencies for the system (19) consisting of $N = 5 \cdot 10^5$ oscillators subject to periodic stimulation with inter-stimulus intervals of length $\tau = 30$. Both, the impact stimuli h_1 with $(\varepsilon, \alpha) = (0.5, 1)$ and the reset stimuli h_2 with $\rho = \pi/8$ are used, and the corresponding $\Omega(\omega)$ are presented in Fig. 11 (a)–(b). The presented structure continues periodically in both directions within the range of the frequency distribution. Note that, oscillators that are locked to $\Omega = 2\pi(z + 1/2)/\tau$ with $z \in \mathbb{Z}$, appear every second stimulus in phase with the stimulus, i.e. constructively contributing to the stimulated pulse. Accordingly, these oscillators introduce a period doubling.

4.2 Impact of the global interaction on the stimulated mode-locked states

By including the global interaction $K > 0$, the width of the locking plateaus corresponding to the locked frequency combs can be increased. This has the effect of increasing the average pulse amplitudes $\left\langle R_1(t_p^+)\right\rangle$. We also find a strong impact of the balancing factor γ on $\left\langle R_1(t_p^+)\right\rangle$, as it is known for the self-organized mode locking.[4]

We perform a numerical simulation, starting from a random uniform initial condition, we stimulate a system with a period $\tau = 30$. The system consists of $N = 5 \cdot 10^5$ oscillators with a fixed random realization of the natural frequencies. After discarding an initial transient of length $25 \cdot 10^3$, we average over $R_1(t_p^+)$, $R_2(t_p^+)$ for an interval of length $150 \cdot 10^3$, and compute the average phase velocities Ω_k. The procedure is repeated for increasing coupling strength K and several values of the balancing parameter γ. For the impact stimulus (9) with $(\varepsilon, \alpha) = (1.0, 1.0)$ the results of the simulation are presented in Fig. 12. In Fig. 12 (a)–(c), one finds $\Omega_k(\omega_k)$ for $\gamma = 1.0, 0.7, 0.5$, respectively. In the absence of the second harmonic coupling $(\gamma = 1)$, the subharmonic plateaus slightly decrease with K, cf. inset in Fig. 12 (a), which, however, does not result in a decrease of $\left\langle R_2(t_p^+)\right\rangle$, see Fig. 12 (e). The largest plateaus shown are harmonic plateaus with $\Omega = 0, \Delta\Omega$ that are widening with increasing K. Accordingly in Fig. 12 (d), one finds a growth of the average pulsation strength $\left\langle R_1(t_p^+)\right\rangle$ with K, which also explains the growth of the $\left\langle R_2(t_p^+)\right\rangle$ at the stimulus times.

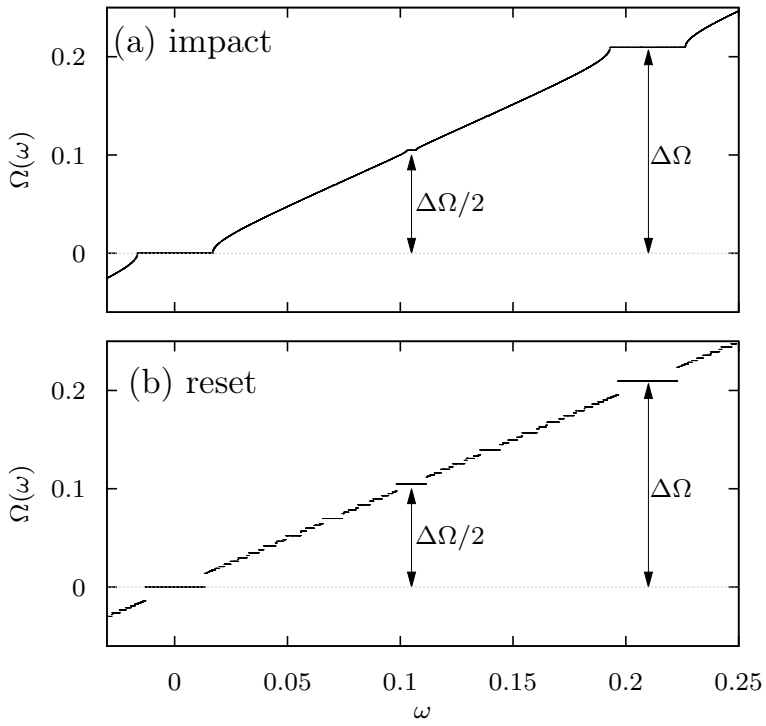

Figure 11: (Color online) Effective frequencies of (19) with $N = 5 \cdot 10^5$, $\tau = 30$, and both the impact stimuli h_1 with $(\varepsilon, \alpha) = (0.5, 1)$ and the reset stimuli h_2 with $\rho = \pi/8$ in (a)–(b), respectively. In (a), the effective frequencies $\Omega(\omega)$ form a Devil's staircase. In (b), the effective frequencies $\Omega(\omega)$ form a discontinuous staircase.

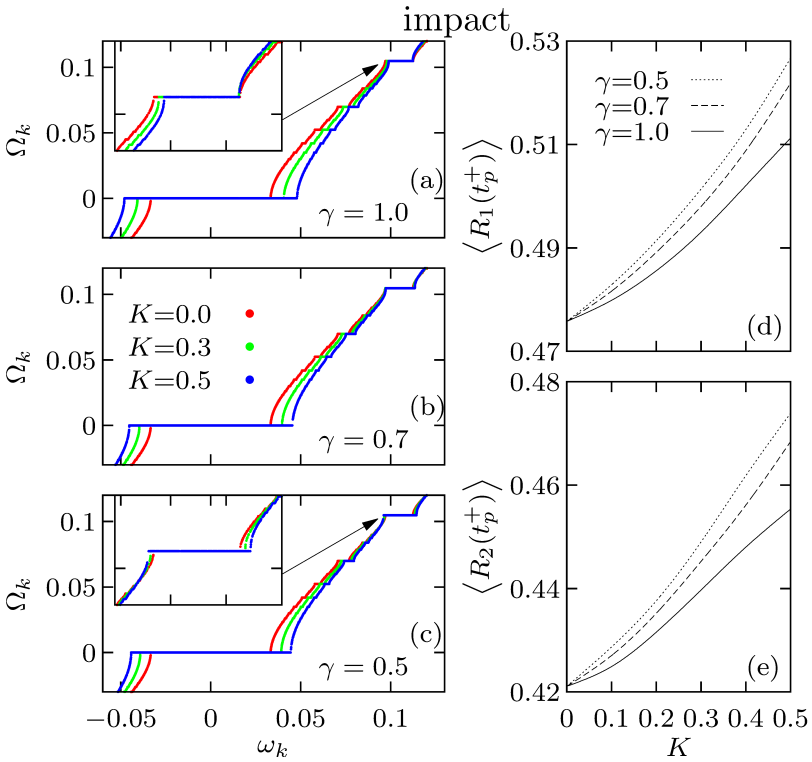

Figure 12: (Color online) Locking plateaus in the average frequencies for varying coupling parameters in system (4) with $N = 5 \cdot 10^5$ oscillators under periodical impact stimulation by (9) with $(\varepsilon, \alpha) = (1.0, 1.0)$ at intervals $\tau = 30$. The resulting averaged pulse amplitudes $\langle R_1(t_p^+)\rangle$, and $\langle R_2(t_p^+)\rangle$ are shown in (d) and (e).

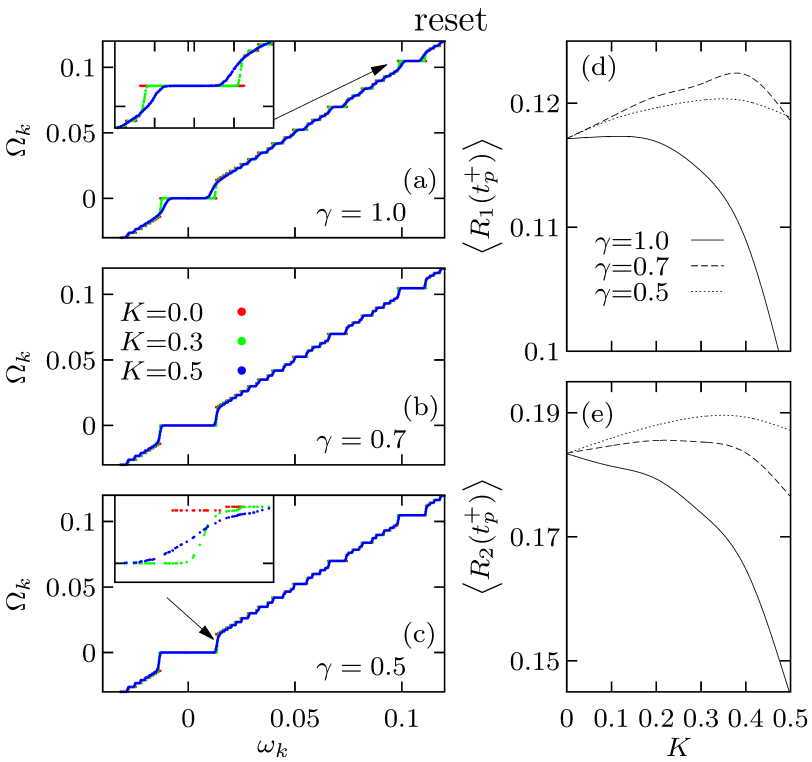

Figure 13: (Color online) Locking plateaus in the average frequencies for varying coupling parameters in system (4) with $N = 5 \cdot 10^5$ oscillators under periodical reset stimulation by (10) with $\rho = \pi/8$ at intervals $\tau = 30$. The resulting averaged pulse amplitudes $\langle R_1(t_p^+)\rangle$, and $\langle R_2(t_p^+)\rangle$ are shown in (d) and (e).

For the reset stimulus (10) with $\rho = \pi/8$, the same procedure is followed and the results are presented in Fig. 13. While the average frequencies $\Omega_k(\omega_k)$ are discontinuous without coupling, one obtians smooth interfaces as soon as the coupling is turned on, cf. Fig. 13 (a)–(c). In absence of the second harmonic coupling $(\gamma = 1)$, the subharmonic plateaus decrease with K, see inset in Fig. 13 (a), which is much less pronounced for $\gamma = 0.5, 0.7$. The largest plateaus shown, are harmonic plateaus with $\Omega = 0, \Delta\Omega$ that are shrinking with K in Fig. 13 (a), while the inset in Fig. 13 (c) reveals a small growth, in particular, for $K = 0.3$. This is reflected by the initial increase of $\langle R_1(t_p^+)\rangle$ with K, cf. Fig. 13 (d), whereas for $\gamma = 1$, one finds an almost immediate degredation of the pulsation strength through the global coupling.

5 Conclusion

The coherence echoes and mode-locked solutions that initially appear as two distinct phenomena are found to be related. In particular, the appearance of the echoes is the result of a mode-locked state induced by the stimulation on a subpopulation of oscillators with natural frequencies on a related comb structure. While the emergence of self-organized mode locking depends on a fixed comb structure of the natural frequencies, the stimulation by two subsequent stimuli acts selectively on an oscillator population with uniform frequency distribution, creating a mode-locked state in a subpopulation with structured natural frequencies. The presence of higher harmonics in the interaction function, which has been shown in [4] to be essential for self-organized mode locking, also has a strong impact on the amplitude of the stimulation induced echoes echoes. For carefully chosen coupling parameters, one can even observe coherence echoes which exceed in amplitude the immediate response to the stimuli.

Another important observation is that the magnitudes of the echoes can occur in a non-monotonous fashion. For the linear model at $K = 0$, the explanation of the nonmonotonic behavior is found in a mutual resonance between the linear (innermodal) dispersion and the reappearance times between echoes which could also be calculated in the continuum limit for the mode-locked initial condition given in Def. 1. By including the global interaction $K > 0$, it is observed that, in particular the first echo increases in magnitude. It turns out that the echo phenomenon is strongly enhanced by the presence of the second harmonic in the coupling function. By considering the order parameters of the oscillators in the mode-locked frequency comb and of the initially unlocked population, we found that the mode-locked population exerts a significant influence on the initially unlocked population where the echoes of the mode-locked initial condition introduce a mode locking on the unlocked population.

For systems with random natural frequencies and periodic stimulation the mode-locked frequency combs are found to successively build up, until a harmonic comb becomes completely locked with the stimulation. In the decoupled case, a reduction to ensembles of circle maps can be made from which the effective frequencies in terms of the rotation numbers of the underlying circle maps can be obtained. In this setting, the presence of subharmonically locked combs can induce a modulation of the stimulated pulsation. As for the self-organized mode locking and the coherence echoes, the global nonlinear interaction with second harmonic coupling $\gamma < 1$ is found to support the stimulated mode-locked states, leading to enhanced average pulse amplitudes.

References

[1] Y. Kuramoto, *Chemical Oscillations, Waves, and Turbulence*, (Springer Series in Synergetics, 1984).

[2] A. Pikovsky, M. Rosenblum, and J. Kurths, *Synchronization: A Universal Concept in Nonlinear Sciences*, (Cambridge university press, Vol. 12., 2003).

[3] O. V. Popovych, Y. L. Maistrenko and P. A. Tass, Phys. Rev. E **71**, 065201(R) (2005).

[4] S. Eydam, and M. Wolfrum, Phys. Rev. E **96**, 052205 (2017).

[5] C. Baesens, J. Guckenheimer, S. Kim, and R. MacKay, Physica D: Nonlinear Phenomena **49**, 387–475 (1991).

[6] Y. H. Wen, M. R. E. Lamont, S. H. Strogatz, and A. L. Gaeta, Phys. Rev. A **94**, 063843 (2016).

[7] H. Taheri, P. Del'Haye, A. A. Eftekhar, K. Wiesenfeld, and A. Adibi, Phys. Rev. A **96**, 013828 (2017).

[8] E. Ott, J. H. Platig, T. M. Antonsen, and M. Girvan, Chaos: An Interdisciplinary Journal of Nonlinear Science **18**, 037115 (2008).

[9] B. Kadomtsev., Sov. Phys. Usp. **11**, 328 (1968).

[10] E. Ott., Journal of Plasma Physics, **4**(3), pp. 471–476 (1970).

[11] R. W. Gould, T. M. O'Neil, and J. H. Malmberg, Physical Review Letters, **19**(5), 219–222 (1967).

[12] E. L. Hahn. Phys. Rev. **80**(4), 580 (1950).

[13] H. Y. Carr, and E. M. Purcell, Physical Review, **94**(3), 630–638 (1954).

[14] T. Chen, M. R. Tinsley, E. Ott, and K. Showalter, Phys. Rev. X **6**, 0461054 (2016).

[15] G. Karras, E. Hertz, F. Billard, B. Lavorel, J.-M. Hartmann, O. Faucher, and I. S. Averbukh, Physical Review Letters, **114**(15) (2015).

[16] H. Daido, Physica D: Nonlinear Phenomena **91**, 24–66 (1996).

[17] D. Hansel, G. Mato, and C. Meunier, Europhysics Letters (EPL) **23**.5: 367–72 (1993).

[18] P. Ashwin, C. Bick, and O. Burylko, Frontiers in Applied Mathematics and Statistics **2** (2016).

[19] M. Komarov, and A. Pikovsky, Phys. Rev. Lett. **111**, 204101 (2013).

[20] H. Chiba, SIAM Journal on Applied Dynamical Systems, SIAM, **16**, 1235–1259 (2017).

[21] A. Katok, and B. Hasselblatt, *Introduction to the modern theory of dynamical systems*, (Cambridge university press, (1997)).

[22] M. H. Jensen, P. Bak, and T. Bohr , Physical Review Letters, **50**(21), 1637–1639 (1983).

[23] J. Guckenheimer, and P. Holmes, *Nonlinear Oscillations, Dynamical Systems and Bifurcatio of Vector Fields*, (Springer, 1983).

[24] R. Brette, Set-Valued Analysis, vol. 11, no. 4 , 359–371 (2003).